論文 / 著書情報
Article / Book Information

Title	Analytical determination of adhesive layer deformation for adhesively bonded double cantilever beam test considering elastic–plastic deformation
Authors	Yu Sekiguchi, Asuka Hayashi, Chiaki Sato
Citation	The Journal of Adhesion, Volume 96, Issue 7, pp. 647-664
Pub. date	2020, 4
Note	This is an Accepted Manuscript of an article published by Taylor & Francis in The Journal of Adhesion on 02/04/2020, available online: http://www.tandfonline.com/10.1080/00218464.2018.1489799.
Note	このファイルは著者（最終）版です。 This file is author (final) version.

Analytical determination of adhesive layer deformation for adhesively bonded double cantilever beam test considering elastic–plastic deformation

Yu Sekiguchi [1,*], Asuka Hayashi [2], Chiaki Sato [1]

[1] Institute of Innovative Research (IIR), Tokyo Institute of Technology, 4259 Nagatsuta-cho, Midori-ku, Yokohama, 226-8503, Japan

[2] Department of Mechanical Engineering, Tokyo Institute of Technology, 4259 Nagatsuta-cho, Midori-ku, Yokohama, 226-8503, Japan

* Corresponding author at: Institute of Innovative Research (IIR), Tokyo Institute of Technology, 4259 Nagatsuta-cho, Midori-ku, Yokohama, 226-8503, Japan.

Tel/Fax: +81-45-924-5012

E-mail address: sekiguchi.y.aa@m.titech.ac.jp (Y. Sekiguchi).

Abstract

The plastic zone at the crack front of an adhesively bonded double cantilever beam (DCB) specimen is analytically expressed considering the deformation of the adhesive layer. The plastic zone length and strain during the crack propagation are obtained, and the effect of the traction–separation profile on the DCB test results is investigated. The fracture energy is given by the area under the traction–separation curve and is not affected by the curve profile. However, the crack length of the DCB specimen is strongly affected by the adhesive deformation, leading to a calculation error in the fracture energy. Therefore, several crack length correction methods have been proposed. An analytical approach to describe the plastic zone at the crack front would help better understand DCB tests for adhesives. In this study, an analytical solution for a DCB test is discussed assuming that the adhesive layer undergoes an elastic–plastic deformation. The elastic zone of the specimen is replaced with a beam on an elastic foundation and the plastic zone with a beam having a uniformly distributed load. Influence of the plastic zone at the crack front in the DCB tests is analytically described by assuming an elastic–perfectly plastic material.

Key words: Analytical models; fracture mechanics; double cantilever beam; traction separation law; strain rate;

Nomenclature

y: Displacement of substrate in vertical direction

x: Coordinate of substrate in horizontal (longitudinal) direction

k: Spring constant

λ: Constant proportional to quarter-power of spring constant

E: Young's modulus of substrate

I: Second moment of inertia of substrate

h: Thickness of substrate

b: Width of substrate

L: Length of substrate

E_a: Young's modulus of adhesive

ν_a: Poison's ratio of adhesive

h_a: Thickness of adhesive

σ_{max}: Maximum stress, or yield stress, of adhesive

ε_a: Strain of adhesive

ε_f: Strain of adhesive at final fracture

α_f: Displacement of adhesive at final fracture

a: Crack length

a_0: Initial crack length

a_e: Effective crack length

Δa: Plastic zone length of adhesive layer

$|\Delta|$: Crack length correction in CBT

P: Applied load

G_{IC}: Adhesive fracture energy, or critical energy release rate, in mode I

δ: Opening displacement

1. Introduction

Adhesive joints are nowadays widely used in many structural parts, including in vehicles such as automobiles, airplanes, and ships. An accurate strength evaluation is essential when the adhesive joints are industrially introduced to new parts. Finite element analyses, such as cohesive zone models, have been used to evaluate the crack propagation problems at the joints [1–5]. The fracture energy is described using a local stress–displacement relationship, namely the traction–separation law. The measurement technique of the adhesive fracture energy using a double cantilever beam (DCB) specimen has been standardized [6, 7]. The DCB test was first analyzed using beam theory considering energy balance [8, 9]. This is a simple model; however, the results, especially the crack length, deviate from the experimental ones. The crack length is strongly affected by the adhesive deformation, leading to a calculation error in the fracture energy. Therefore, the difference between the theoretical crack length and the measured one was investigated, and the crack length correction in the corrected beam theory (CBT) [10–13] and an effective crack length, namely compliance-based beam method (CBBM), [14, 15] have been respectively derived. Replacing the adhesive layer with an elastic foundation, i.e., the Winkler foundation, closed form solutions were obtained for the DCB [15–18] and other test methods [19, 20]. However, generally, the adhesive at the crack front deforms

plastically because of the stress concentration. Additionally, some adhesives are designed to behave elastic–perfectly plastic (non–hardened elasto–plastic) in order to enhance energy absorption performance. These adhesives are composed of several different polymers, and material characteristics change with loading rate. Thus, the fracture energy shows rate dependency. Conversely, it is difficult to experimentally measure strain rate of the adhesive layer because of its thinness. An analytical approach to describe the plastic zone at the crack front would help better understand DCB tests, especially rate dependency, for such adhesives. Williams and Hadavinia discussed the non–elastic effect using various traction–separation profiles by extending the beam on an elastic foundation model [21]. Additionally, Yamada proposed an analytical solution considering the elastic–plastic deformation of the adhesive layer [22, 23]. This concept was applied to other analytical models [24, 25]. In the solution, the plastically deformed adhesive region was replaced with a uniformly distributed load, which can be employed when the adhesive is assumed elastic–perfectly plastic. In this paper, this concept is extended to analyze deformation and strain rate of the adhesive layer accompanied by the crack propagation in DCB specimens, and the effect of the traction–separation profile on the DCB test results is discussed.

2. DCB model

2.1 Traction separation law

A triangular form is widely used as a profile for the traction–separation law. A trapezoidal form with a constant stress stage is also used, especially for ductile adhesives [26, 27]. Figure 1 shows the stress–strain relation of a second–generation acrylic (SGA) structural adhesive (C355-20 A/B, Denka Co., Ltd., Tokyo Japan) with a tensile test using bulk specimens at a cross head speed of 1 mm/min. This adhesive elongate around 60% with flat stress stage. For such kind of adhesives, it would be suitable to employ the trapezoidal profile, shown in Fig. 2, which is of an elastic–perfectly plastic. In the case of the triangular form, only damage process contribute to a fracture process zone (FPZ) at a crack front. Conversely, plastic deformation process also contribute to the FPZ in the case of the trapezoidal form. Especially when the plastic range is wide like the mentioned adhesive, contribution of the plasticity to the FPZ is considered to be larger. Therefore, damage process is neglected for simplification in this study.

In the mentioned trapezoidal form, the adhesive first deforms linear-elastically. When the stress at the crack front reaches $\sigma_{\max}$, a plastic zone is generated. A fracture occurs when the displacement at the crack front reaches α_{f}.

2.2 Model configuration

An adhesively bonded DCB specimen is considered, as shown in Fig. 3a. The elastically deformed adhesive layer is converted to a parallel spring arrangement (see Fig. 3b). The plastically deformed adhesive layer is converted to a uniformly distributed load (see Fig. 3c). Although the spring constant for adhesively bonded parts can be defined in several different ways [15–20], a spring constant assuming the deformation of the adhesive under a plane strain state, given as

$$k = \frac{(1-\nu_a)}{(1-2\nu_a)(1+\nu_a)}\frac{E_a b}{h_a}, \quad (1)$$

is employed. In the calculation process, only the upper half of the deformation is considered owing to the symmetry (see Fig. 3b). Thus, the adhesive layer with a spring constant k is replaced with a direct connection of two springs with a spring constant k_{half}, where $1/k = 2/k_{\mathrm{half}}$.

2.3 Formulation

The adhesive layer is first elastically deformed (first step) by applying a load to the end of the DCB specimen (see Appendix). With the increase in the opening displacement, the stress at the crack front soon reaches the maximum stress, i.e., the yield stress. At this point, the adhesive is plastically deformed around the crack front. The plastic zone length

increases with further increase in δ (second step). The deformation of the adhesive at the crack front then reaches α_{f}, and the crack begins to propagate (third step).

When the crack front of the adhesive layer is plastically deformed (the second and third steps), the deformation of the substrate can be divided into three zones; a crack zone with no adhesion, a plastic zone around the crack front and an elastic zone. The crack zone can be assumed as a cantilever beam, the plastic zone as a beam with a uniformly distributed load and the elastic zone as a beam on an elastic foundation. The substrate deformations are given as

$$Y_{\mathrm{c}} = A_{\mathrm{c}}X^3 + B_{\mathrm{c}}X^2 + C_{\mathrm{c}}X + D_{\mathrm{c}} \quad (2)$$

for the crack zone ($X < 1$);

$$Y_{\mathrm{p}} = W_{\max}X^4 + A_{\mathrm{p}}X^3 + B_{\mathrm{p}}X^2 + C_{\mathrm{p}}X + D_{\mathrm{p}} \quad (3)$$

for the plastic zone ($1 < X < 1 + \Delta A$); and

$$Y_{\mathrm{e}} = e^{\lambda'(1+\Delta A-X)}(A_{\mathrm{e}} \cos \lambda'(1 + \Delta A - X) + B_{\mathrm{e}} \sin \lambda'(1 + \Delta A - X)) \quad (4)$$

for the elastic zone ($1 + \Delta A < X$), where ΔA and $W_{\max}$ are normalized as $\Delta A = \Delta a/a$ and $W_{\max} = \sigma_{\max}a^3/24EI$, respectively. Ten unknown coefficients and the plastic zone length are obtained by satisfying the boundary conditions at $X = 0$, $Y_{\mathrm{c}} = D$, and $\mathrm{d}^2Y_{\mathrm{c}}/\mathrm{d}x^2 = 0$; continuity conditions at $X = 1$, $Y_{\mathrm{c}} = Y_{\mathrm{p}}$, $\mathrm{d}Y_{\mathrm{c}}/\mathrm{d}x = \mathrm{d}Y_{\mathrm{p}}/\mathrm{d}x$, $\mathrm{d}^2Y_{\mathrm{c}}/\mathrm{d}x^2 = \mathrm{d}^2Y_{\mathrm{p}}/\mathrm{d}x^2$, and $\mathrm{d}^3Y_{\mathrm{c}}/\mathrm{d}x^3 = \mathrm{d}^3Y_{\mathrm{p}}/\mathrm{d}x^3$; and continuity conditions

at $X = 1 + \Delta A$, $Y_{\mathrm{p}} = Y_{\mathrm{e}}$, $\mathrm{d}Y_{\mathrm{p}}/\mathrm{d}x = \mathrm{d}Y_{\mathrm{e}}/\mathrm{d}x$, $\mathrm{d}^2Y_{\mathrm{p}}/\mathrm{d}x^2 = \mathrm{d}^2Y_{\mathrm{e}}/\mathrm{d}x^2$, $\mathrm{d}^3Y_{\mathrm{p}}/\mathrm{d}x^3 = \mathrm{d}^3Y_{\mathrm{e}}/\mathrm{d}x^3$, and $\mathrm{d}^4Y_{\mathrm{p}}/\mathrm{d}x^4 = \mathrm{d}^4Y_{\mathrm{e}}/\mathrm{d}x^4$. The results are given as follows.

$$A_{\mathrm{c}} = 4W_{\max} + A_{\mathrm{p}}, \quad (5)$$

$$B_{\mathrm{c}} = 0, \quad (6)$$

$$C_{\mathrm{c}} = 4W_{\max} + C_{\mathrm{p}}, \quad (7)$$

$$D_{\mathrm{c}} = D, \quad (8)$$

$$A_{\mathrm{p}} = -\frac{2W_{\max}}{\lambda'}\left(l_{\mathrm{a}} + 1 + \frac{\lambda'^2}{l_{\mathrm{a}}+1}\right), \quad (9)$$

$$B_{\mathrm{p}} = 6W_{\max}, \quad (10)$$

$$C_{\mathrm{p}} = \frac{2W_{\max}}{\lambda'^3}\left\{{l_{\mathrm{a}}}^3 + 3{l_{\mathrm{a}}}^2 + 3(1-\lambda'^2)(l_{\mathrm{a}}+1)\right\}, \quad (11)$$

$$D_{\mathrm{p}} = W_{\max} + D, \quad (12)$$

$$A_{\mathrm{e}} = -6W_{\max}/\lambda'^4, \quad (13)$$

$$B_{\mathrm{e}} = \frac{6W_{\max}}{\lambda'^4}\left(\frac{\lambda'^2}{l_{\mathrm{a}}+1} - l_{\mathrm{a}}\right), \quad (14)$$

and

$${l_{\mathrm{a}}}^5 + 5{l_{\mathrm{a}}}^4 + (10-2\lambda'^2){l_{\mathrm{a}}}^3 + (12-6\lambda'^2){l_{\mathrm{a}}}^2 + \left\{12 - 6\lambda'^2 + \frac{D_{\mathrm{p}}\lambda'^4}{W_{\max}}\right\} l_{\mathrm{a}} + 6 + \frac{D_{\mathrm{p}}\lambda'^4}{W_{\max}} = 0, \quad (15)$$

where $l_{\mathrm{a}} = \lambda'(1 + \Delta A)$. By solving Eq. (15) for l_{a}, for example using the newton method, the plastic zone length can be obtained.

In the first and second steps, the crack front remains at $a = a_0$. The values of all the

variables can then be determined using δ. Conversely, the crack propagation needs to be considered in the third step. In this case, a becomes an additional variable. Therefore, another condition is required to determine the values of all the variables. When the crack propagates, the displacement at the crack front is equal to α_{f}. Adding this condition, the crack propagation of the DCB specimen can be described.

3. Experimental

The DCB test substrates consisting of spring steel (grade "SUP10") with the width 24.8 mm and the length 187.0 mm were used. The surface of the substrates were sandblasted with Al_2O_3 abrasives and wiped with acetone before bonding. The thickness of the substrate was measured after the sandblasting as 1.77 mm. The SGA structural adhesive (C355-20 A/B, Denka Co., Ltd., Tokyo Japan) was used. Curing condition was 24 °C for 1 day and then 60 °C for 2 hours. The adhesive layer thickness was measured as 0.31 mm by subtracting the thickness of the substrates measured before the specimen manufacturing from the total thickness of the specimen. A polytetrafluoroethylene (PTFE) film was inserted to create initial crack. The initial crack length was measured by the side view image as 54 mm. Because only single PTFE film was inserted, obtuse crack front was created. Therefore, results of initial stage of the crack propagation was removed

from the fracture energy calculation. The fracture test of the DCB specimen was conducted in a material testing machine (STB-1225S, A&D Co., Ltd., Tokyo Japan) at a crosshead speed of 5 mm/min. The crack length was measured with a CCD camera. The specimen was cohesively fractured in whole area (see Fig. 4).

4. Results and discussion

4.1 Analytical solutions

The DCB test was first analytically conducted with substrate parameters $E = 207$ GPa, $h = 2$ mm, $b = 24.8$ mm and $L = 180$ mm, and with adhesive parameters $E_{\mathrm{a}} = 500$ MPa, $\nu_{\mathrm{a}} = 0.37$, $\sigma_{\max} = 10$ MPa, $\varepsilon_{\mathrm{f}} = 0.6$, and $h_{\mathrm{a}} = 0.3$ mm (denoted as case 1). Thus, $\alpha_{\mathrm{f}} = \varepsilon_{\mathrm{f}} h_{\mathrm{a}} = 0.18$ mm. The adhesive parameters are derived based on the tensile test results (see Fig. 1). The initial crack length was set to $a_0 = 50$ mm.

Figure 5 shows the load–displacement curve. The plastic deformation at the crack front is observed from a relatively early stage in the load increasing region. The load decreasing region with crack propagation is in a good agreement with the results of the conventional DCB theory, which is expressed using the simple beam theory as

$$P = \left(\frac{4}{9} E I b^3 G_{\mathrm{IC}}^3 \frac{1}{\delta^2}\right)^{1/4}. \quad (16)$$

Figure 6 shows the variation in the crack length. Figure 7 shows the plastic zone length

with comparison of $a_e - a$ and $|\Delta|$. Although the effective crack length for the CBBM is originally obtained using a shear corrected beam theory [14], shear effect on the cantilever deformation is negligibly small for the analyzed condition. Therefore, it is obtained using the simple beam theory as

$$a_e = \sqrt[3]{\frac{3EI\delta}{2P}}, \quad (17)$$

in this study. The crack length correction is obtained using a plot of cube root of the compliance versus the crack length according to the CBT [6]. From these results, the increase in the plastic zone length before the crack propagation is confirmed. In contrast, the plastic zone length is largely constant during the fracture. Additionally, the corrections regarding the crack length are found to be largely in good agreement with the plastic zone length. Therefore, it is confirmed that crack length deviation due to the plastic zone is correctly incorporated in the correction term.

The fracture energy of the analytical DCB test obtained by the CBT is $G_{IC} = 1.78$ kJ/m^2. Likewise, the fracture energy obtained by integrating the traction–separation curve under the given condition is also 1.78 kJ/m^2. Therefore, it is confirmed that the proposed analytical solution can describe the crack propagation of the DCB specimen from the viewpoint of the fracture energy.

Figure 8 shows the relationship between ε_a and δ at $x =$ 50, 51, 55, 65, 75, 100, 125,

150, and 175 mm. The strain smoothly increases at the initial crack point (i.e., $x = 50$ mm). Because Δa is approximately 7.0 mm, the adhesive layer when $x < a_0 + \Delta a \approx 57$ mm is plastically deformed before the start of the crack propagation. In this range, a discontinuous change in the slope is observed at the start of the crack propagation (see arrows in Fig. 8). In the remaining range, i.e., $x > a_0 + \Delta a$, the strain increases smoothly after some compression. The gradient of the curves of the ε_a–δ relationship is related to the strain rate because of the relationship

$$\frac{d\varepsilon_a}{d\delta} = \frac{d\varepsilon_a}{dt} / \frac{d\delta}{dt}. \quad (18)$$

Figure 9 shows the relationship between $d\varepsilon_a/d\delta$ and δ. The strain rate monotonically increases for the most part with respect to the crack propagation. The maximum strain rate increases by approximately four times as the crack propagation begins, as shown by an arrow in Fig. 9, though local crack propagation and micro crack generation at the crack front would prevent such a rapid increase in practice. Conversely, the maximum strain rate decreases with the increase in the crack length. For the quasi–static test, the opening displacement speed is generally set under 5 mm/min. When $d\delta/dt = 5.0$ mm/min, the strain rate is in the range of approximately $1.7–4.2 \times 10^{-2}$ s^{-1}, which is close to the strain rate of the quasi–static tensile tests for bulk specimens. On the other hand, the opening displacement speed is significantly higher for the dynamic DCB tests, and is a

few meters per second or more [28–30]. When $d\delta/dt = 2.0$ m/s, the strain rate is in the range of approximately 400–1000 s^{-1}, which is a value applied to high-speed crash tests. However, with regard to the strain rate, the change in the traction–separation law needs to be considered. Additionally, the behavior of adhesives at high strain rates is very complicated. Therefore, a careful discussion is required for the analysis of the strain rate effect. Recently, digital image correlation (DIC) method is rapidly developing and is used for the analysis of adhesive layer deformation [31]. If the resolution of the image can be increased enough to analyze the deformation of thin adhesive layer, as well as the movement of the crack propagation can be followed with the images, the DIC could be one of the solutions for the experimental analysis of the strain rate effect.

The fracture energy is given by the area under the traction-separation curve and is not related to the curve profile. Conversely, the profile is important when the deformation of the adhesive layer needs to be considered. Here, two additional forms of the traction–separation relationship, as shown in Fig. 10, are considered. Following are the conditions to unify the area under the curves: case 2 for $E_a = 2000$ MPa, $\nu_a = 0.37$, $\sigma_{max} = 20$ MPa, and $\varepsilon_f = 0.3$; and case 3 for $E_a = 125$ MPa, $\nu_a = 0.37$, $\sigma_{max} = 5$ MPa, and $\varepsilon_f = 1.2$. Because the fracture energy is the same, the load–displacement curves at the crack propagation stage coincide with each other. Conversely, the curves at the load

increasing stage without the crack propagation differ, as shown in Fig. 11; the gradient increases for higher aspect ratio profile (case 2) and decreases for lower one (case 3). Moreover, the difference in the profiles affected the plastic zone length and the strain rate. The average Δa changed from 7.0 (case 1) to 4.9 (case 2) and 10.0 mm (case3). Figure 12 shows the maximum strain rate at each point. Interestingly, the points well fit with the function $f(x) = cx^{0.9}$ for each case with different values of c, where c is a coefficient, though a clear physical interpretation cannot be made. The plastic zone is longer and the strain rate is higher for the adhesive having a flatter trapezoidal form of the traction–separation relationship given the same fracture energy.

4.2 Experimental results and discussion

The fracture energy of the prepared specimen calculated by the CBT was 2.21 kJ/m^2, which was larger than the value obtained from the traction–separation relationship determined from the tensile test. Test condition was almost plane stress stage for the tensile test using the bulk specimens, and it was plane strain stage for the DCB test. This difference could be one of the reasons for the mismatch of the traction–separation relationship. Polymers, including adhesives, highly depend on the loading rate, which could be another reason. Conversely, it has been confirmed that system compliance effect

was small enough to be neglected. Whatever the reasons, it is necessary to reconfigure the traction–separation relationship. Figure 13 shows the traction–separation relationship where $\sigma_{\max}$ and α_{f} are adjusted so that the area under the curves becomes 2.2 kJ/m^2. When the traction–separation profile is changed, the plastic zone length changes as mentioned above. Figure 14 shows the plastic zone length variation against $\sigma_{\max}$ in the case of $G_{\mathrm{IC}} = 2.2$ kJ/m^2 for the tested condition. From the experimental results, $a_{\mathrm{e}} - a$ and $|\Delta|$ are obtained as 6.7 and 6.1 mm, respectively. Therefore, the maximum stress at the crack front is approximately same or slightly increases compared to the tensile test, and it is confirmed that there is no significant change in $\sigma_{\max}$ and α_{f}. Figure 15 shows the load-displacement relationship in the case of the traction–separation relationship with $\sigma_{\max} = 12$ MPa. Analyzed and experimental results well agreed each other at the crack propagation part because the fracture energy obtained from the experimental results was employed for the analysis. Additionally, the results at the initial part with no crack propagation also coincide well. Thus, it is indicated that inverse estimation of the traction–separation relationship from Δa works effectively.

5. Conclusion

An analytical solution for a DCB test is derived assuming the substrate of the specimen

as a beam on an elastic foundation for the region in which the adhesive is elastically deformed and as a beam with a uniformly distributed load for the region in which the adhesive is plastically deformed. Although a trapezoidal form of the traction–separation relationship is assumed, the traction–separation profile varies depending on the type of adhesives, and some of them have hardening and/or damaging processes. Therefore, the analytical result can only compare with the experimental ones when the actual profile does not deviate so much from the assumption. Conversely, the tendency of the plastic zone effect on the DCB test results can be predicted by using the proposed solution. The load–displacement relationship during the crack propagation is in good agreement with the conventional DCB theory. The length of the plastically deformed area and the strain of the adhesive layer are directly obtained at an arbitrary point. The proposed solution can analytically describe the effect of the profile on the plastic zone length and strain when the same fracture energy is employed in the trapezoidal traction–separation relationship. Additionally, the traction–separation relationship at the crack front can be predicted by comparing the relationship between the plastic zone length and the trapezoidal shape with the experimental results.

Appendix

When the entire adhesive layer is elastically deformed (the first step), the deformation of the substrate can be divided into two zones: a crack zone with no adhesion and an elastic zone. The substrate deformations are given as

$$Y_{\mathrm{c}} = A_{\mathrm{c}}X^3 + B_{\mathrm{c}}X^2 + C_{\mathrm{c}}X + D_{\mathrm{c}} \quad (19)$$

for the crack zone ($X < 1$), and as

$$Y_{\mathrm{e}} = e^{\lambda'(1-X)}(A_{\mathrm{e}} \cos \lambda'(1-X) + B_{\mathrm{e}} \sin \lambda'(1-X)) \quad (20)$$

for the elastic zone ($X > 1$), where Y, X, and λ' are normalized as $Y = y/a$, $X = x/a$, and $\lambda' = a\lambda$, respectively, with $\lambda = (k_{\mathrm{half}}/EI)^{1/4}/\sqrt{2}$. Six unknown coefficients are obtained by satisfying the boundary conditions at $X = 0$, $Y_{\mathrm{c}} = D$, and $\mathrm{d}^2Y_{\mathrm{c}}/\mathrm{d}x^2 = 0$ and continuity conditions at $X = 1$, $Y_{\mathrm{c}} = Y_{\mathrm{e}}$, $\mathrm{d}Y_{\mathrm{c}}/\mathrm{d}x = \mathrm{d}Y_{\mathrm{e}}/\mathrm{d}x$, $\mathrm{d}^2Y_{\mathrm{c}}/\mathrm{d}x^2 = \mathrm{d}^2Y_{\mathrm{e}}/\mathrm{d}x^2$, and $\mathrm{d}^3Y_{\mathrm{c}}/\mathrm{d}x^3 = \mathrm{d}^3Y_{\mathrm{e}}/\mathrm{d}x^3$. The results are given as follows.

$$A_{\mathrm{c}} = \frac{\lambda'^3}{(2\lambda'^3+6\lambda'^2+6\lambda'+3)}, \quad (21)$$

$$B_{\mathrm{c}} = 0, \quad (22)$$

$$C_{\mathrm{c}} = -\frac{3(\lambda'+1)^2 A_{\mathrm{c}}}{\lambda'^2}, \quad (23)$$

$$D_{\mathrm{c}} = D, \quad (24)$$

$$A_{\mathrm{e}} = A_{\mathrm{c}} + C_{\mathrm{c}} + D, \quad (25)$$

and

$$B_{\mathrm{e}} = \frac{3A_{\mathrm{c}}}{\lambda'^2}, \quad (26)$$

where D is normalized as $D = \delta/2a$.

References

[1] Blackman, B. R. K.; Hadavinia, H.; Kinloch, A. J.; Williams, J. G. The use of a cohesive zone model to study the fracture of fibre composites and adhesively-bonded joints. *Int. J. Fract.* 2003, **119**, 25–46. DOI: 10.1023/A:1023998013255.

[2] Alfano, M.; Furgiuele, F.; Leonardi, A.; Maletta, C.; Paulino, G. H. Mode I fracture of adhesive joints using tailored cohesive zone models. *Int. J. Fract.* 2009, **157**, 193–204. DOI: 10.1007/s10704-008-9293-4.

[3] Matzenmiller, A.; Gerlach, S.; Fiolka, M. A critical analysis of interface constitutive models for the simulation of delamination in composites and failure of adhesive bonds. *J. Mech. Mater. Struct.* 2010, **5**, 185–211. DOI: 10.2140/jomms.2010.5.185.

[4] Chaves, F. J. P.; de Moura, M. F. S. F.; da Silva, L. F. M.; Dillard, D. A. Numerical analysis of the dual actuator load test applied to fracture characterization of bonded joints. *Int. J. Solids. Struct.* 2011, **48**, 1572–1578. DOI: 10.1016/j.ijsolstr.2011.02.006.

[5] Abe, N.; Sekiguchi, Y.; Sato, C. Parameter identification of material model of toughened adhesive polymer for elasto–plastic finite element analysis. *J. Adhes. Soc. Jpn.*

In press 2018.

[6] ISO, Adhesives –Determination of the mode 1 adhesive fracture energy of structural adhesive joints using double cantilever beam and tapered double cantilever beam specimens. ISO Standard, 2009; ISO 25217.

[7] ASTM D3433-99. Standard test method for fracture strength in cleavage of adhesives in bonded metal joints, (American Society for Testing and Materials, West Conshohocken, Re-approved in 2012).

[8] Gilman, J. J. Direct measurements of the surface energies of crystals. *J. Appl. Phys.* 1960, **31**, 2208–2218. DOI: 10.1063/1.1735524.

[9] Gills, P. P.; Gilman, J. J. Double cantilever cleavage mode of crack propagation. *J. Appl. Phys.* 1964, **35**, 647–658. DOI: 10.1063/1.1713430.

[10] Hashemi, S.; Kinloch, A. J.; Williams, J. G. Corrections needed in double-cantilever beam tests for assessing the interlaminar failure of fibre-composites. *J. Mater. Sci. Lett.* 1989, **8**, 125–129. DOI: 10.1007/BF00730701.

[11] Williams, J. G. End corrections for orthotropic DCB specimens. *Compos. Sci. Technol.* 1989, **35**, 367–376. DOI: 10.1016/0266-3538(89)90058-4.

[12] Blackman, B.; Dear, J. P.; Kinloch, A. J.; Osiyemi, S. The calculation of adhesive fracture energies from double-cantilever beam test specimens. *J. Mater. Sci. Lett.* 1991,

10, 253–256. DOI: 10.1007/BF00735649.

[13] Blackman, B. R. K.; Kinloch, A. J.; Paraschi, M.; Teo, W. S. Measuring the mode I adhesive fracture energy, GIC, of structural adhesive joints: the results of an international round-robin. *Int. J. Adhes. Adhes.* 2003, **23**, 293–305. DOI: 10.1016/S0143-7496(03)00047-2.

[14] de Moura, M. F. S. F.; Morais, J. J. L.; Dourado, N. A new data reduction scheme for mode I wood fracture characterization using the double cantilever beam test. *Eng. Fract. Mech.* 2008, **75**, 3852–3865. DOI: 10.1016/j.engfracmech.2008.02.006.

[15] Sekiguchi, Y.; Katano, M; Sato, C. Experimental study of the mode I adhesive fracture energy in DCB specimens bonded with a polyurethane adhesive. *J. Adhes.* 2017, **93**, 235–255. DOI: 10.1080/00218464.2015.1070101.

[16] Kanninen, M. F. An augmented double cantilever beam model for studying crack propagation and arrest. *Int. J. Fract.* 1973, **9**, 83–92. DOI: 10.1007/BF00035958.

[17] Penado, F. E. A closed form solution for the energy release rate of the double cantilever beam specimen with an adhesive layer. *J. Compos. Mater.* 1993, **27**, 383–407. DOI: 10.1177/002199839302700403.

[18] Jiang, Z.; Wan, S.; Li, M.; Ma, L. Analytical solution for non-uniformity of energy release rate of orthotropic double cantilever beam specimens with an adhesive layer. *Eng.*

Fract. Mech. 2016, **164**, 46–59. DOI: 10.1016/j.engfracmech.2016.07.011.

[19] Budzik, M.; Jumel, J.; Imielinska, K.; Shanahan, M. E. R. Effect of adhesive compliance in the assessment of soft adhesives with the wedge test. *J. Adhes. Sci. Technol.* 2011, **25**, 131–149. DOI: 10.1163/016942410X501133.

[20] Williams, M. L. The fracture threshold for an adhesive interlayer. *J. Appl. Poly. Sci.* 1970, **14**, 1121–1126. DOI: 10.1002/app.1970.070140501.

[21] Williams, J. G.; Hadavinia, H. Analytical solutions for cohesive zone models. *J. Mech. Phys. Solids* 2002, **50**, 809–825. DOI: 10.1016/S0022-5096(01)00095-3.

[22] Yamada, S. E. Elastic/plastic fracture analysis for bonded joints. *Eng. Fract. Mech.* 1987, **27**, 315–328. DOI: 10.1016/0013-7944(87)90149-4.

[23] Yamada, S. E. The J-integral for augmented double cantilever beams and its application to bonded joints. *Eng. Fract. Mech.* 1988, **29**, 673–682. DOI: 10.1016/0013-7944(88)90169-5.

[24] Erpolat, S.; Ashcroft, I. A.; Crocombe, A. D.; Wahab, M. A. On the analytical determination of strain energy release rate in bonded DCB joints. *Eng. Fract. Mech.* 2004, **71**, 1393–1401. DOI: 10.1016/S0013-7944(03)00163-2.

[25] Plaut, R. H.; Ritchie, J. L. Analytical solutions for peeling using beam-on-foundation model and cohesive zone. *J. Adhes.* 2004, **80**, 313–331. DOI:

10.1080/00218460490445832.

[26] Tvergaard, V.; Hutchinson, J. W. On the toughness of ductile adhesive joints. *J. Mech. Phys. Solids* 1996, 44, 789–800. DOI: 10.1016/0022-5096(96)00011-7.

[27] Campilho, R. D. S. G.; de Moura, M. F. S. F.; Domingues, J. J. M. S. Using a cohesive damage model to predict the tensile behaviour of CFRP single-strap repairs. *Int. J. Solids Struct.* 2008, **45**, 1497–1512. DOI: 10.1016/j.ijsolstr.2007.10.003.

[28] Blackman, B. K. R.; Kinloch, A. J.; Sanchez, F. S. R.; Teo, W. S.; Williams, J. G. The fracture behaviour of structural adhesives under high rates of testing. *Eng. Fract. Mech.* 2009, **76**, 2868–2889. DOI: 10.1016/j.engfracmech.2009.07.013.

[29] Yamagata, Y.; Sekiguchi, Y.; Sato, C. Experimental investigation of mode I fracture energy of adhesively bonded joints under impact loading conditions. *Appl. Adhes. Sci.* 2017, **5**, 7. DOI: 10.1186/s40563-017-0087-7.

[30] Sekiguchi, Y.; Yamagata, Y.; Sato, C. Mode I fracture energy of adhesive joints bonded with adhesives with different characteristics under quasi-static and impact loading. *J. Adhes. Soc. Jpn.* 2017, **53**, 330–337.

[31] Kawasaki, S; Sekiguchi, Y; Nakajima, G; Haraga, K; Sato, C. Digital image correlation measuring of strain and stress distribution on mixed adhesive joints bonded by honeymoon adhesive using two types of second-generation acrylic adhesives of two

components. *J. Adhes. Soc. Jpn.* 2017, **53**, 192-201.

Figures

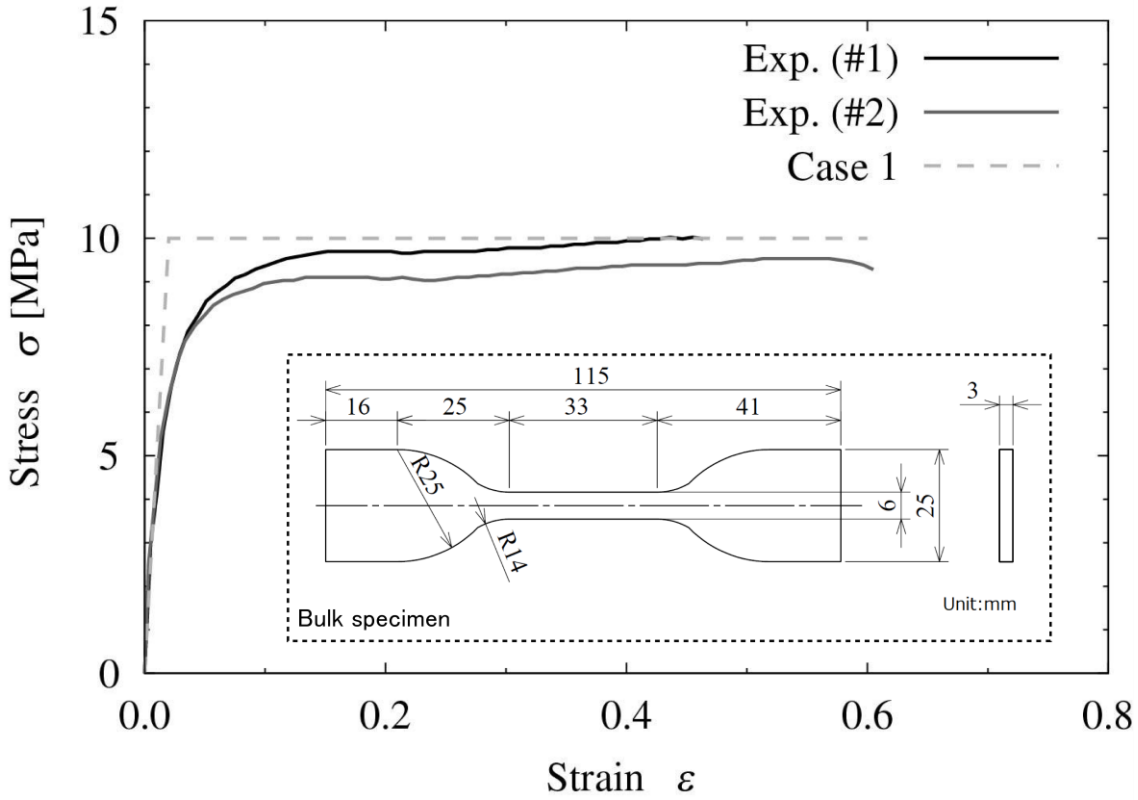

Figure 1. Experimentally obtained stress–strain curves of SGA adhesive and stress–strain relation for case 1.

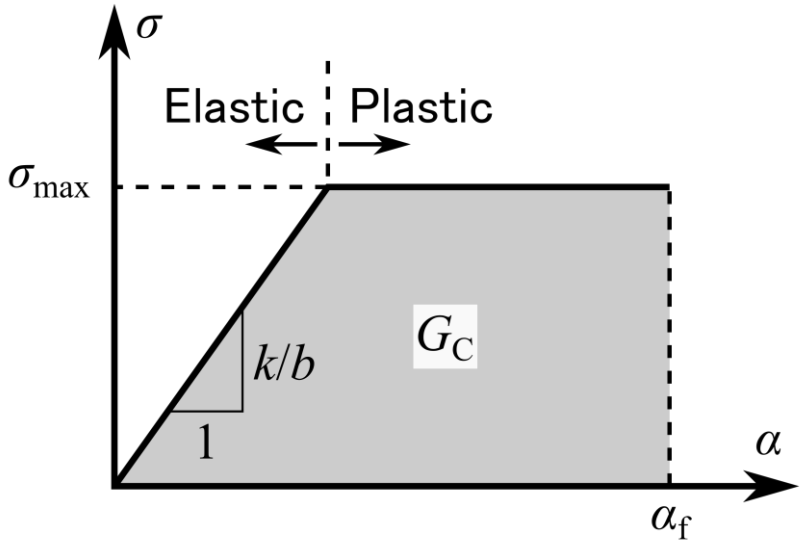

Figure 2. Trapezoidal form of the traction–separation relationship where σ and α are the stress and the displacement of adhesive, and fracture energy G_C is given by the area under the curve.

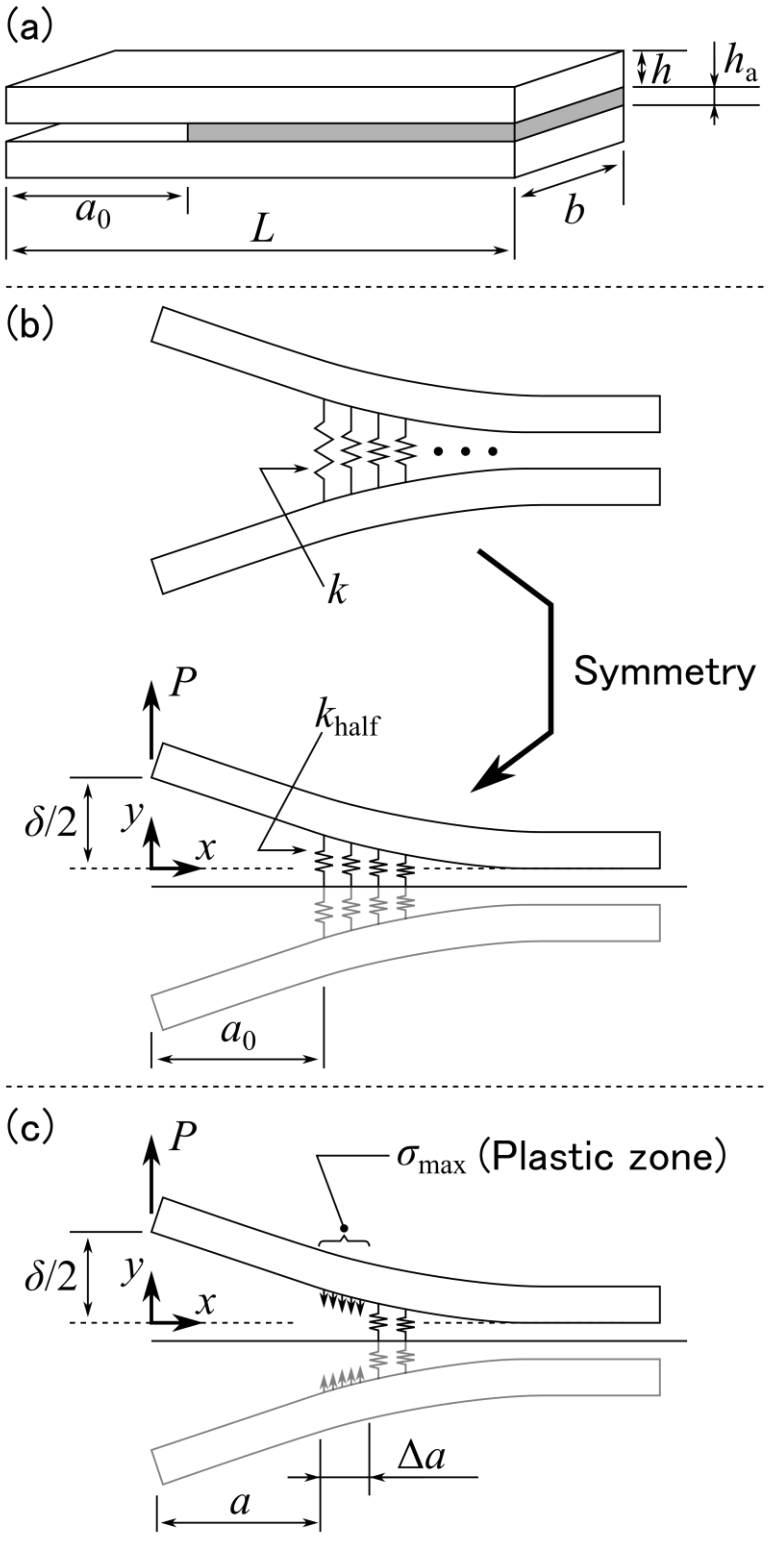

Figure 3. Schematics of (a) a DCB specimen, (b) a model for elastic deformation of adhesive layer, and (c) a model for elastic-plastic deformation of adhesive layer.

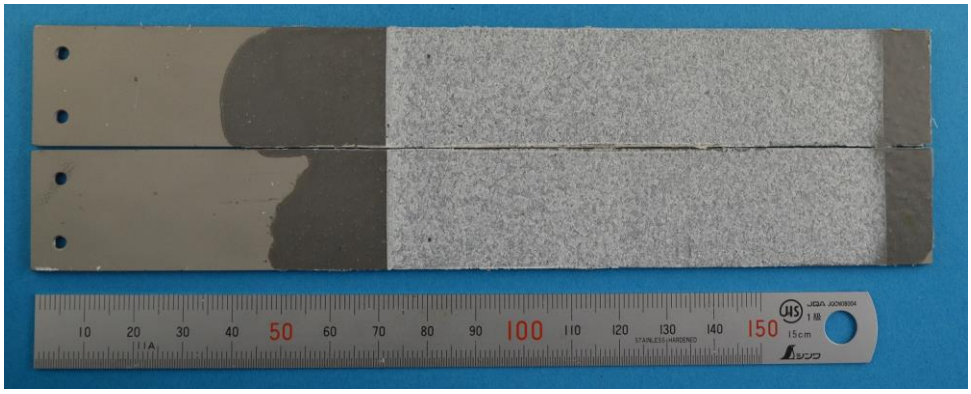

Figure 4. Fracture surfaces for the DCB test specimen with the SGA adhesive.

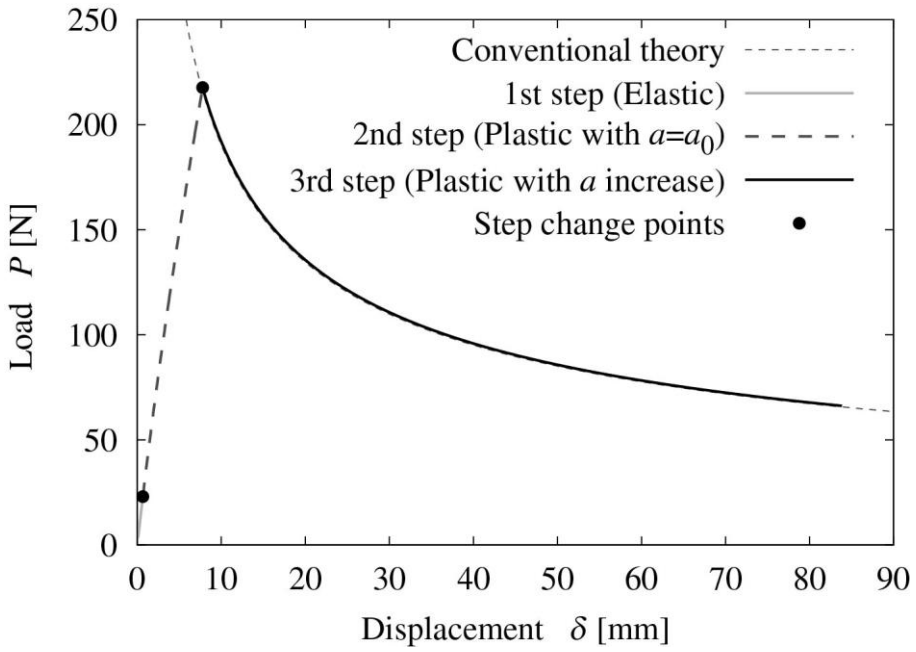

Figure 5. Analytically obtained load–displacement curve of DCB test.

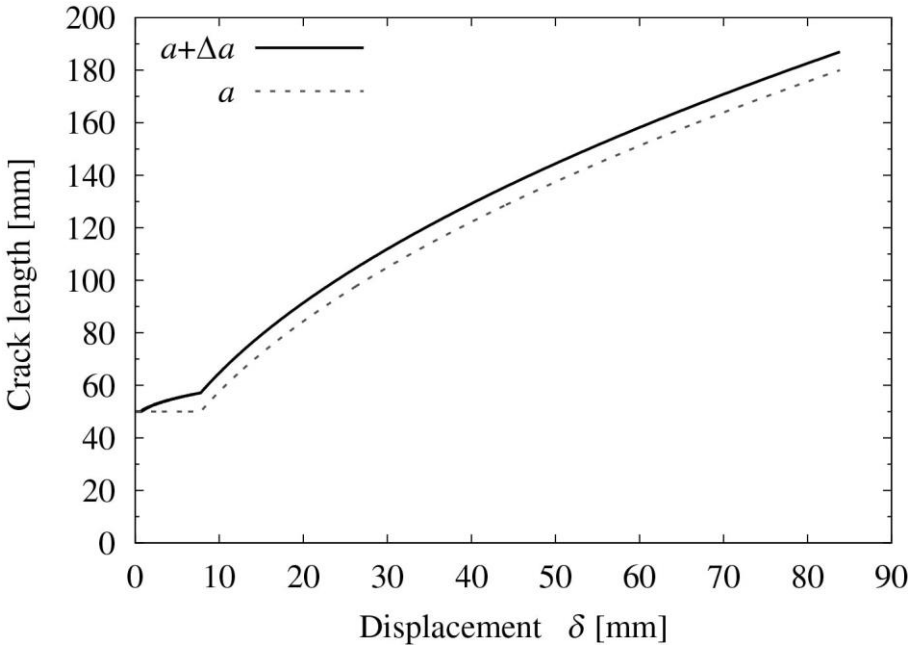

Figure 6. Analytically obtained variations in the crack length with and without the plastic zone length with respect to displacement.

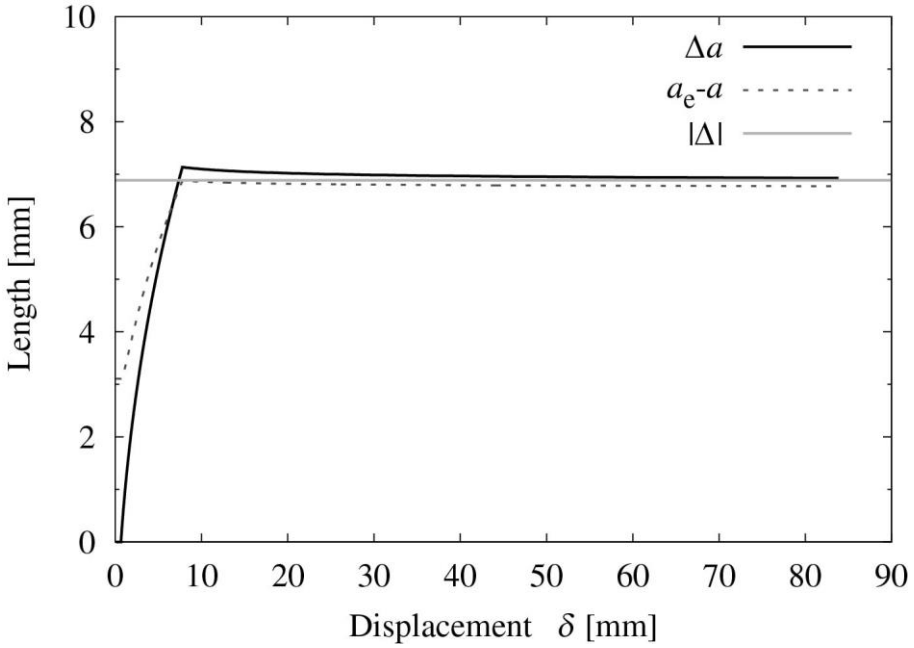

Figure 7. Analytically obtained variations in the plastic zone length (Δa), the difference between the effective crack length and the crack length ($a_e - a$), and the crack length

correction (|Δ|) with respect to the displacement.

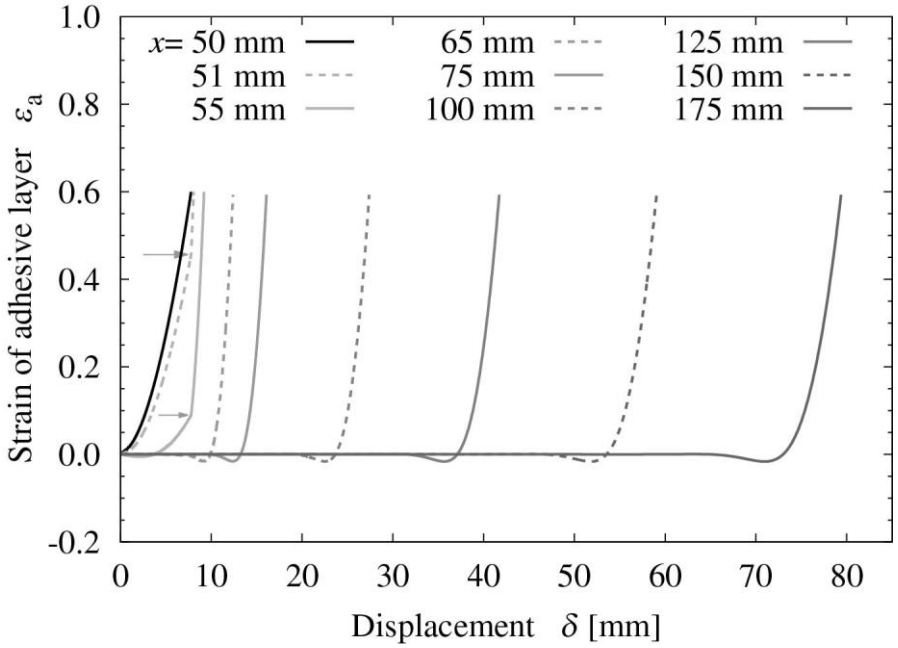

Figure 8. Analytically obtained strain of the adhesive layer with respect to the displacement at various points. The arrows indicate the start point of the crack propagation.

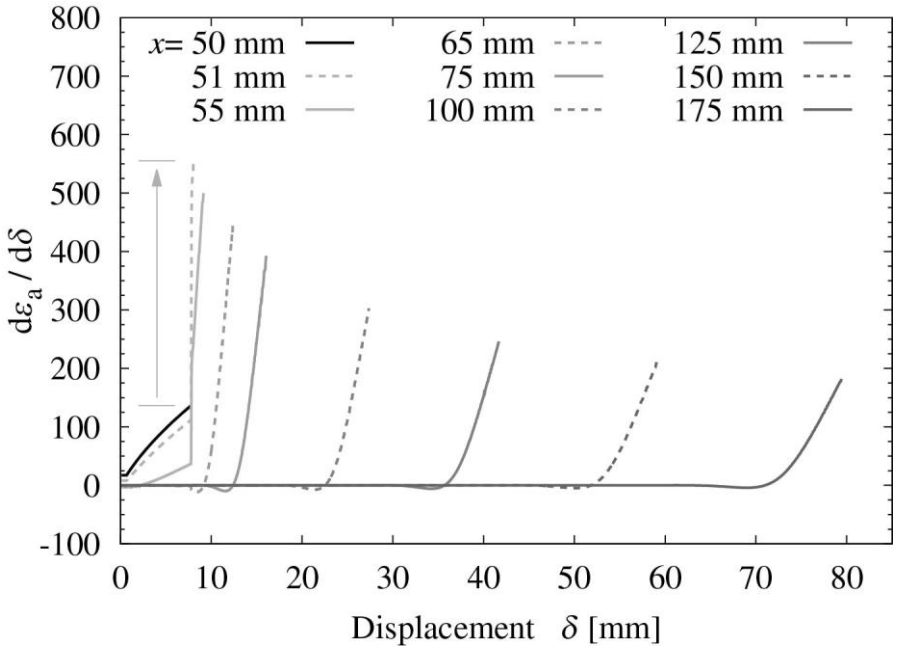

Figure 9. Analytically obtained $d\varepsilon_a/d\delta$ versus displacement for various points.

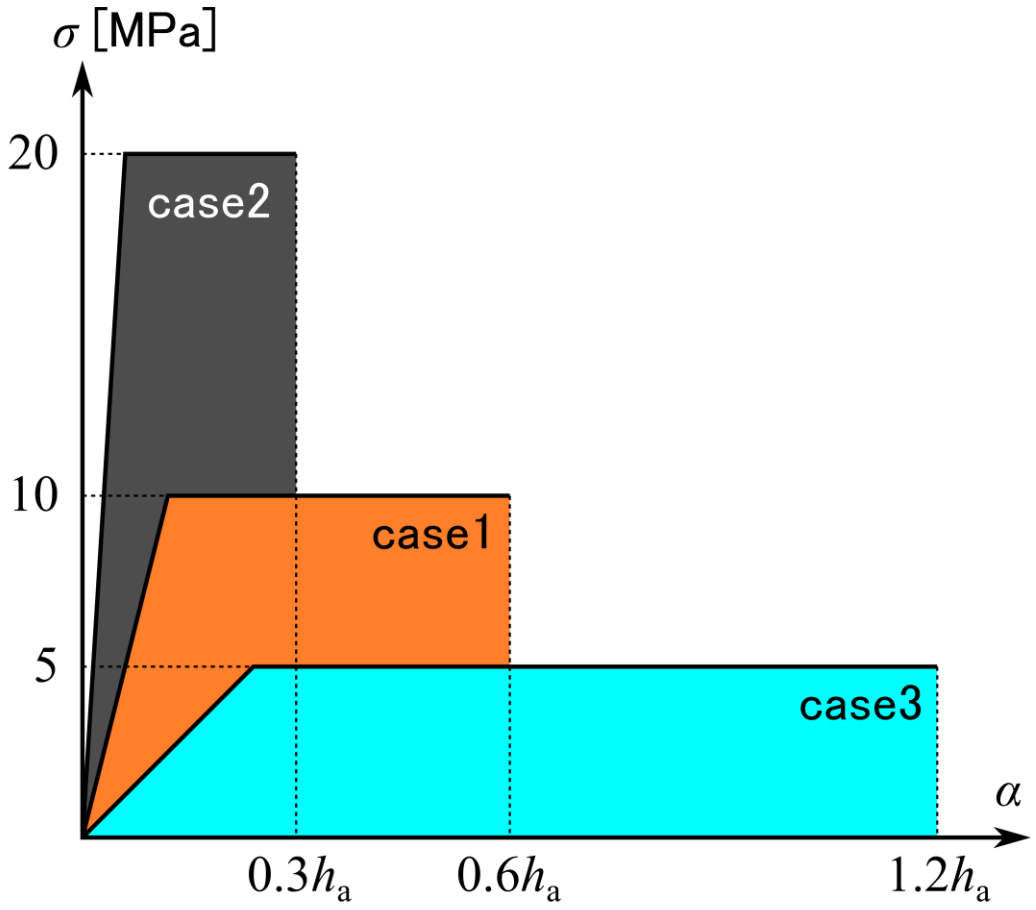

Figure 10. Three types of traction–separation profiles with the same area under the curves.

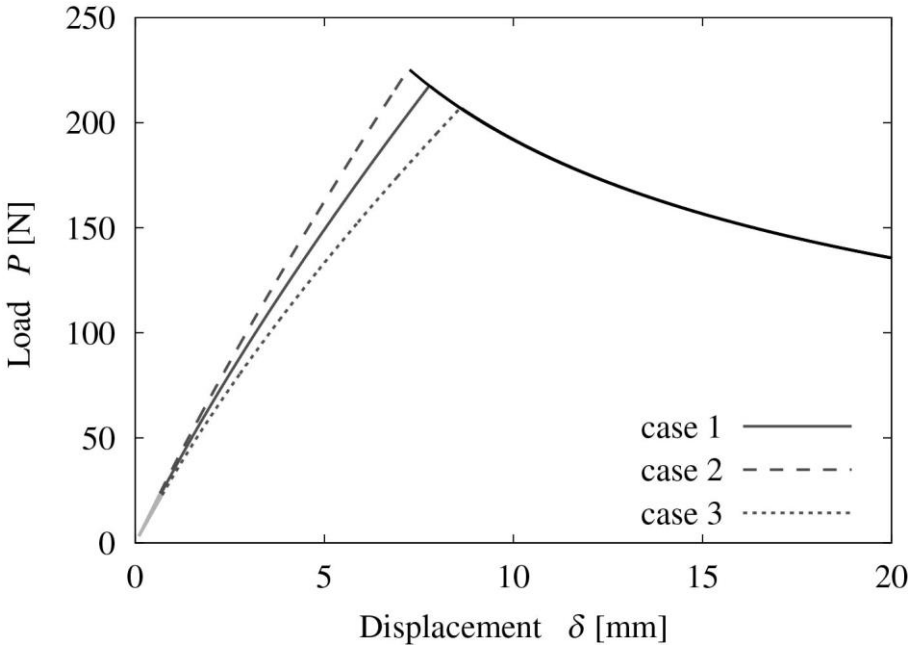

Figure 11. Analytically obtained load–displacement curves with different types of traction–separation relationships.

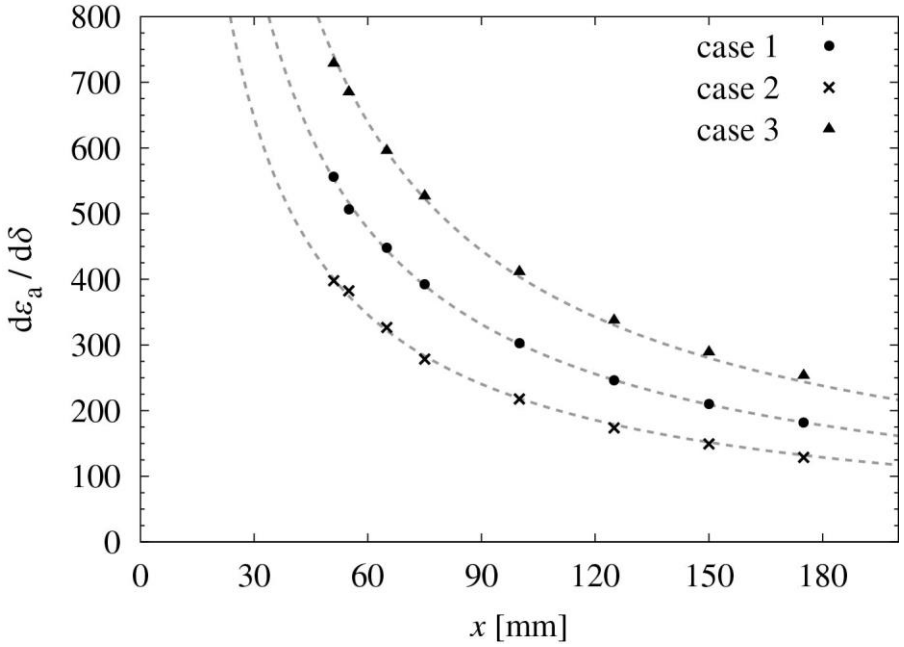

Figure 12. Analytically obtained maximum $d\varepsilon_a/d\delta$ versus x with different types of traction–separation relationships.

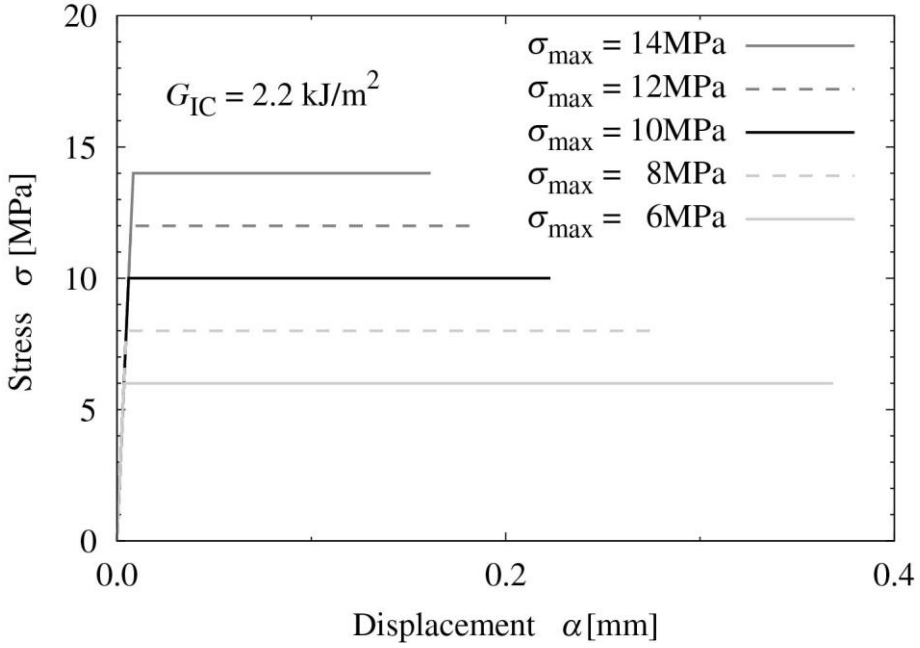

Figure 13. Traction–separation relationships for $G_{IC} = 2.2$ kJ/m^2 with different σ_{max} and α_f.

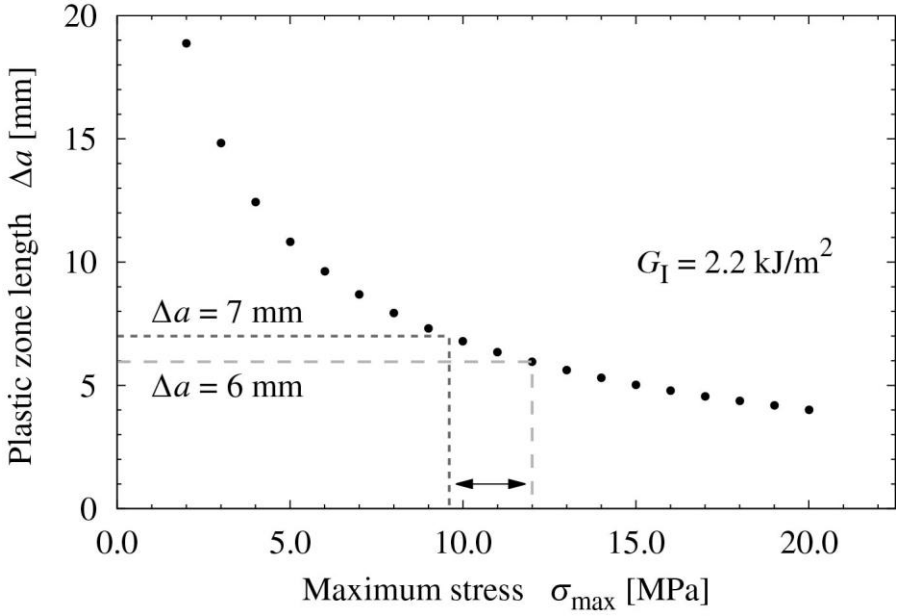

Figure 14. Analytically obtained relationship between plastic zone length and maximum stress in the case of $G_{IC} = 2.2$ kJ/m^2 for the tested condition.

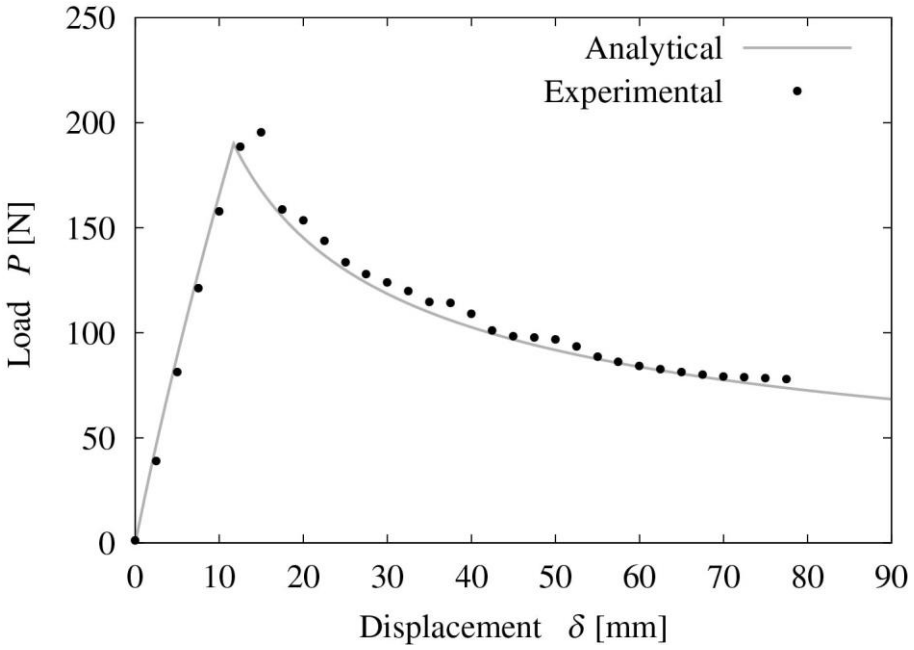

Figure 15. Load–displacement relationship of the experimental results and the analytical result in the case of the traction-separation relationship with $\sigma_{\max} = 12$ MPa.